Non-monochromatic laser assist scattering in thermal environment

Saddam Husain Dhobi [ID][a,*], Kishori Yadav[b], Suresh Prasad Gupta[b], Jeevan Joyti Nakarmi[a], Ajay Kumar Jha[c]

[a]*Central Department of Physics, Tribhuvan University, Kirtipur 44618, Nepal*
[b]*Department of Physics, Patan Multiple Campus, Tribhuvan University, Lalitpur 44700, Nepal*
[c]*Department of Mechanical and Advance Engineering, Institute of Engineering, Pulchowk Campus, Tribhuvan University, Lalitpur 44700, Nepal*

Abstract

This study aims to investigate the differential cross-section (DCS) in a non-monochromatic laser-assisted thermal environment. Building on existing research, which primarily explores electron dynamics and ionization processes without considering thermal effects, this work seeks to bridge this research gap by examining the DCS under non-monochromatic laser fields in a thermal environment. The methodology involves utilizing a vector potential derived by Milosvic to represent non-monochromatic laser fields and applying a semi-classical approximation with the help of Volkov solutions. The S-matrix is then obtained to study the DCS. The developed model was computed to analyze the nature of the DCS. The results indicate that the DCS for photon absorption is higher than for emission due to atomic oscillation/excitation. This causes atom expansion upon absorption and a decrease in field strength during emission. Furthermore, the DCS behavior varies with the phase of the non-monochromatic wave and polarization, with distinct patterns observed for absorption and emission scenarios. The DCS with energy at different rates of absorption and emission exhibits a damping nature. Additionally, the DCS shows oscillatory behavior with separation distance, displaying higher values for absorption and varying with laser phase. The findings provide valuable insights into electron-atom interactions under laser fields in thermal conditions, with implications for quantum thermal machines, photochemistry, proton exchange membrane fuel cells (PEMFC), and more.

Communicated by: B. J. Falaye

1. Introduction

Laser control of nuclear motion in molecules is advancing, with improved laser technology offering pulses with controllable amplitude and phase. This enables coherent control scenarios to manipulate photochemical products via superpositions of electronic or nuclear states. Electron control in atoms has been successful through phase manipulation between two laser fields, influencing angular distributions of photoelectrons in ionization processes or directing photocurrents in quantum wells, which are analogous to molecular systems. Such superpositions also enable control of ionization and enhance high-order harmonic generation [1]. Zhang and Nakajima [2] stud-

---

*Corresponding author Tel.: +97-980-810-00285

Email addresses: saddam@ran.edu.np (Saddam Husain Dhobi [ID]),
yadavkishori70@gmail.com (Kishori Yadav)

ied Coulomb effects on photoionization of hydrogen atoms with circular and linearly polarized intense laser fields, finding that Coulomb fields affect ionization dynamics based on photoelectron momentum, particularly in linearly polarized fields. However, they did not explore DCS or thermal environments for scattering.

Schnez *et al.* [3] applied a fully relativistic quantum electrodynamic approach using Volkov solutions and Dirac-Volkov propagators to study cross sections for spontaneous bremsstrahlung emission in circular and linear laser fields, where classical ponderomotive energies exceed the electron's rest mass. Jin *et al.* [4] found that multiple interference structures in xenon atom photoelectron momentum distributions (PMDs) can be manipulated using two-color laser fields, influenced by forward-scattered electrons due to Coulomb effects. Adjusting the relative phase of the two colors can enhance or suppress these structures. Jin *et al.* [5] investigated nonsequential double ionization (NSDI) in IR+XUV fields, noting that forward collisions dominate when electrons are ejected in the same direction, while both forward and backward collisions contribute comparably when ejected oppositely.

Yu *et al.* [6] used the Coulomb-Volkov distorted-wave approximation (CVA) to study electron momentum distributions in orthogonally polarized two-color pulses, finding better agreement with experimental observations compared to strong-field approximation (SFA) simulations, due to different Coulomb phase corrections. Richter *et al.* [7] demonstrated control over electron momentum distributions from single ionization of Ar using two orthogonally polarized laser pulses of different colors, showing that the visibility of interference fringes depends on the controllable phase between the pulses. Buică [8, 9] examined DCS in laser-assisted (e,2e) processes and fast-electron-impact ionization in hydrogen atoms but did not consider thermal effects. Dhobi *et al.* [10–12] investigated DCS in weak laser fields, designed a Volkov wave function to study thermal electron scattering, and explored DCS with the Volkov-Thermal Wave Function in Coulomb potential.

After reviewing the literature, it is observed that research to date has not comprehensively addressed non-monochromatic laser-assisted scattering in a thermal environment, focusing instead on monochromatic or two- and three-color laser fields without considering thermal effects on DCS. Existing studies, such as those by Bandrauk and Chelkowski [1], Zhang and Nakajima [2], Schnez *et al.* [3], and Jin *et al.* [4], primarily explore electron dynamics and ionization processes but overlook the thermal environment's impact. Dhobi *et al.* [10–12] have investigated DCS in various contexts but not specifically within a thermal setting. This work aims to fill this gap by examining DCS under non-monochromatic laser fields in a thermal environment, thereby providing novel insights into electron-atom interactions influenced by laser parameters and thermal conditions. This research will significantly advance the understanding of laser-matter interactions, with potential applications. Specifically, our work on temperature control in proton exchange membrane fuel cells (PEMFCs) relates to advances in quantum thermal machines, where managing heat at the nanoscale is vital for improving device efficiency. By examining how non-monochromatic radiation affects heat dissipation, our research can inform the development of more efficient quantum devices, such as quantum refrigerators and heat engines.

2. Materials and method

To study the DCS for thermal electron in non-monochromatic laser assisted. We consider the vector potential design by Milosvic as shown in equation (1). The theory can be easily generalized to a laser field with an arbitrary vector potential $\mathbf{A}(t)$ and, the vector potential of a N-colour elliptically polarized laser field has the form [13]

$$\mathbf{A}(t) = A_0 \sum_{n=1}^{N} \left[a_n \Big(\Lambda_{1n} \cos(n\omega t + \phi_n) + \Lambda_{2n} \sin(n\omega t + \phi_n) \Big) \right], \tag{1}$$

where a_n, $n\omega$, and ϕ_n are the relative amplitude (with a being the ratio of field strength) [14], frequency, and phase (phase $\phi = 0, \pi/4, \pi/2, 3\pi/4$, and π) of the nth vector potential component. The polarization of the nth component is defined by the vectors $\Lambda_{1n} = \hat{e}_1 \cos \zeta_n$ and $\Lambda_{2n} = \hat{e}_2 \sin \zeta_n$. For $\zeta_n = 0$, the nth component is linearly polarized, while for $\zeta_n = \pi/4$, the polarization is circular. A_0 is the equal field amplitude [15], $a = \frac{E_0}{\omega}$, where E_0 is the magnitude of the electric field, and $I = \frac{1}{2} c \epsilon_0 E_0^2 \Rightarrow E_0 = \left(\frac{2I}{c\epsilon_0} \right)^{1/2}$. The most notable gauges in strong-field physics beyond the dipole approximation are the Lorentz-gauge and the Coulomb gauge [16]. The wave function of an electron in laser field is expressed in equation (2) is also known as Volkov wave function;

$$X(r, t) = \frac{1}{(2\pi)^{3/2}} \exp \left\{ i \frac{\mathbf{p}}{\hbar} \cdot \left(r + \frac{e}{m} \int \mathbf{A}(t) \, dt \right) - i \frac{E}{\hbar} t - i \frac{e^2}{2m\hbar} \int \mathbf{A}^2(t) \, dt \right\}. \tag{2}$$

Substituting value of $\mathbf{A}(t)$ from equation (1) in equation (2) and solving for thermal case using superposition theorem. The the obtained equation (3) is the wave function of laser assist electron in thermal environment for elliptical polarized,

$$\begin{aligned} X^E(r, t) = {} & \frac{1}{(2\pi)^{3/2}} \exp \{ i\mathbf{p} \cdot r \\ & + \sum_{n=1}^{N} \left(\frac{i a_n \alpha_0 \mathbf{p} \sin(n\omega t + \phi_n - \gamma)}{n} \right) -iEt \} \\ & - k_e \nabla T_{eT} \exp(i\omega_e T t), \end{aligned} \tag{3}$$

where $\alpha_0 = eA_0/m\omega$ and $\tan \gamma \implies \tan \theta \tan \zeta_n$ and $\gamma \implies \tan^{-1}(\tan \theta \tan \zeta_n)$. Also, the last term of equation (2) is neglected because it tends to zero when operated with its complex conjugate. Similarly, for non-monochromatic linear polarization, the Volkov wave function for a thermal electron [12]

$(\Lambda_{1n} = \hat{e}_1 \cos\zeta_n$ and $\Lambda_{2n} = \hat{e}_2 \sin\zeta_n = 0)$ is obtained from equation (1) and equation (2), for $\cos\zeta_n = 1$, we get:

$$X^L(r, t) = \frac{1}{(2\pi)^{3/2}} \exp\left\{ i\mathbf{p} \cdot r \right.$$
$$+ i\mathbf{p} \cdot \alpha_0 \sum_{n=1}^{N} \frac{a_n}{n} \sin(n\omega t + \phi_n)$$
$$- iEt - i\frac{\alpha_0}{4} \sum_{n=1}^{N} \frac{a_n}{n} \left(n\omega t + \frac{\sin(2n\omega t + 2\phi_n)}{2} \right) \right\}$$
$$- k_e \nabla T_e T \exp(i\omega_e T t). \tag{4}$$

For Non-monochromatic elliptical and circular polarized in thermal environment transition matrix using Kroll and Watson approximation using equation (5) shown below

$$S = \delta_{fi} - \int \langle X_f | V(r) | X_i \rangle, \tag{5}$$

where X_i and X_f represent the initial and final wave functions of a non-monochromatic wave. By substituting the value of X^{EC} from equation (3) into equation (5) and solving, we obtain the following expression for $V(r) = 4\zeta(3)/3\pi\beta^3 r^2 - 4\zeta(5)/5\pi\beta^5 r^4$ [17]. The thermal potential is then given by:

$$T_{fi}^E = J_l \left(\sum_{n=1}^{N} \frac{a_n \alpha_0 q \cos\theta}{n} \right) \exp il(\phi_n - \gamma) f_{\text{Born}}^{(1)}$$
$$- k_e \left(\nabla T_{eiT} + \nabla T_{efT} \right) \frac{\delta(\omega_{efT} - \omega_{eiT})}{\delta(E_{efT} - E_{eiT} + nl\omega)}. \tag{6}$$

Equation (6) represents the transition matrix used to calculate the DCS for non-monochromatic elliptical waves. The first term involves a Bessel function J_l, with a sum over quantum states n and phase factors $\exp[il(\phi_n - \gamma)]$, combined with the Born approximation $f_{\text{Born}}^{(1)}$. This allows for a simplified, analytic treatment of scattering processes under weak interactions. The second term includes ∇T and Dirac delta functions that enforce energy and frequency conservation, enabling the analysis of thermal effects on energy transitions. Together, these components model quantum transitions with thermal dependence while ensuring adherence to conservation laws, which is crucial for understanding temperature-dependent processes in fields such as spectroscopy, materials science, and energy systems. The Born factor is given by equation (7):

$$f_{\text{Born}}^{(1)} = -\frac{4\pi}{q} \left[-\frac{4\zeta(3)}{3\pi\beta^3} \left(\frac{\exp(iqr)\left(-iq^3r^3 + 3q^2 + 6iqr - 6\right)}{q^4} \right.\right.$$
$$\left. + \frac{\exp(-iqr)\left(iq^3r^3 + 3q^2 - 6iqr - 6\right)}{q^4} \right)$$
$$- \frac{4\zeta(5)}{5\pi\beta^5} \left(\frac{\exp(-iqr)\left(iq^5r^5 + 5q^4r^4 - 20iq^3r^3\right)}{q^6} \right.$$
$$+ \frac{\exp(-iqr)\left(-60q^2r^2 + 120iqr + 120\right)}{q^6}$$
$$+ \frac{\exp(iqr)\left(-iq^5r^5 + 5q^4r^4 + 20iq^3r^3\right)}{q^6}$$
$$\left.\left. - \frac{\exp(iqr)\left(60q^2r^2 + 120iqr - 120\right)}{q^6} \right)\right]. \tag{7}$$

Equation (7) accounts for the various contributions to the Born factor, incorporating terms involving $\exp(i\mathbf{qr})$ and $\exp(-i\mathbf{qr})$, along with their associated coefficients.

For the absorption and emission of a photon from the non-monochromatic laser field, the DCS is given by:

$$\left(1 \mp \frac{l\omega}{p_i^2} \right)^{1/2} = \frac{p_f}{p_i}$$
$$\left(\frac{d\sigma}{d\Omega} \right)_E = \left(1 \mp \frac{l\omega}{p_i^2} \right)^{1/2} \left(T_{fi}^E \right)^2. \tag{8}$$

Equation (8) represents the DCS for photon absorption and emission. The term $\left(1 \mp \frac{l\omega}{p_i^2} \right)^{1/2}$ serves as a modification factor that depends on the initial momentum p_i, the photon's frequency ω, and l, which represents the number of absorbed or emitted photons. The factor $\left(T_{fi}^E \right)^2$ is the transition matrix element for the electric field case.

Additionally, for the non-monochromatic circular polarization case, we have $\gamma \implies \tan^{-1}(\tan\theta \tan\zeta_n)$. Taking $\tan\zeta_n = 1$, we obtain $\gamma \implies \tan^{-1}(\tan\theta)$. Thus, the DCS becomes:

$$\left(\frac{d\sigma}{d\Omega} \right)_c = \left(1 \mp \frac{l\omega}{p_i^2} \right)^{1/2} \left(T_{fi}^C \right)^2. \tag{9}$$

Equation (9) represents the general form but specifically applies to non-monochromatic circular polarization, with T_{fi}^C being the corresponding transition matrix element. A similar DCS for non-monochromatic linear polarization is obtained, as shown in equation (10).

$$\left(\frac{d\sigma}{d\Omega} \right)_L = \left(1 \mp \frac{l\omega}{p_i^2} \right)^{1/2} \left(T_{fi}^L \right)^2, \tag{10}$$

where,

$$T_{fi}^L = J_l \left(\frac{1}{n} \sum_{n=1}^{N} a_n \alpha_0 q \cos\theta \right) \exp(il\phi_n) f_{\text{Born}}^{(1)}$$
$$- k_e \left(\nabla T_{eiT} + \nabla T_{efT} \right) \frac{\delta\left(\omega_{efT} - \omega_{eiT}\right)}{\delta\left(E_{efT} - E_{eiT} + nl\omega\right)}. \tag{11}$$

The theoretical model developed in this work is validated through experiments conducted on a single PEMFC, where the exothermic reaction creates a thermal environment. In this environment, the generated electrons, protons, and hydrogen atoms around the PEMFC electrode contribute to current and voltage generation. The thermal environment consists of a mixture of different wavelengths, resulting from the collisions of electrons, protons, and hydrogen atoms, particularly in bulk systems or stacks. This interaction within the thermal environment is crucial for understanding the performance of the PEMFC.

3. Result and discussion

3.1. DCS with non-monochromatic elliptical and circular

The DCS for photon absorption from a non-monochromatic laser field is higher than for photon emission, as shown in Figure 1. This is because, when an atom absorbs a photon, it undergoes expansion due to the internal vibrations of its electrons,

and the atom oscillates, covering a larger area of interaction with the incident photon. In contrast, during photon emission, the atom undergoes much smaller expansion and oscillation, resulting in a reduced area of interaction. Additionally, during photon emission, the field strength of the atom decreases as it transitions to a lower energy state, causing the incoming electron's field to dominate. This leads to a stronger Coulomb interaction between the atom and the projected electron, bringing them closer together, which results in a lower DCS.

On the other hand, photon absorption increases the field strength (due to the Coulomb interaction) between the incident electron and the target atom, leading to greater deflection as a result of the Coulomb charge interactions between the target and the projected electron. As a result, the DCS is higher for photon absorption. This pattern holds true for both positive and negative ellipticities ($\pi/2$ and $-\pi/2$). Compared to monochromatic laser-assisted scattering, where the DCS decreases as noted by Buica [18], the non-monochromatic laser-assisted scattering in this work shows a higher DCS for absorption due to the complex interactions introduced by the variable characteristics of the laser field. Figure 1 illustrates the DCS for photon absorption and emission at various non-monochromatic laser phases. The DCS for absorption is higher when the laser phase is π, indicating more superposition between photons and electrons in the presence of the target. In contrast, at phase zero, where no superposition occurs, the DCS is lower. Generally, the DCS increases with the phase of the applied photons for absorption. In the emission case, the DCS is higher at phase π, but lower at phase $\pi/4$. This suggests that the interaction range for absorption is greater, and the probability of interaction between particles is higher at laser phase $\pi/4$, whereas other phases show lower probabilities.

Comparing the DCS for emission and absorption at the same phase reveals that the DCS for absorption is consistently higher than for emission. DeHarak *et al.* [19] studied the effects of polarization direction on laser-assisted free-free scattering, finding that the DCS as a function of scattering angle is symmetric in nature. Moreover, the DCS for non-monochromatic elliptical polarization is higher than for non-monochromatic circular polarization, and the DCS for non-monochromatic circular polarization is higher than for non-monochromatic linear polarization. This is because elliptical polarization covers a larger area in the x-y plane during travel, increasing the probability of interaction. Circular polarization covers a smaller area, and linear polarization covers an even smaller, single-direction area, resulting in the lowest DCS. Jablonski *et al.* [20] found that, for hydrogen atoms, the DCS as a function of scattering angle follows a sinusoidal wave pattern in the absence of a laser field, which aligns with the general behavior observed in other studies.

Figure 2 shows how the DCS decreases with increasing incidence energy of the electron for both the absorption and emission of a single photon. In Figure 2(a), the absorption scenario is depicted, while Figure 2(b) shows the emission scenario. This decrease in DCS is attributed to the Bessel function, a mathematical function derived from the Volkov wave function, which represents the effect of the laser field on a free electron.

The Bessel function induces oscillations in the DCS, reflecting the oscillating component of the electron's velocity and energy during the scattering event. This behavior was similarly observed in the absorption of photons [21]. For both emission and absorption, the DCS is higher at a laser phase of π compared to phases zero and $\pi/4$, with similar trends observed for ellipticity $-\pi/2$. Additionally, while the DCS for non-monochromatic circular polarization is less than for non-monochromatic elliptical polarization, it remains higher than for non-monochromatic linear polarization. The larger interaction area in the x-y plane for non-monochromatic elliptical polarization results in a higher probability of interaction, explaining the higher DCS compared to both non-monochromatic circular and non-monochromatic linear polarizations.

In the case of photon absorption, the DCS exhibits lower damping compared to the emission scenario. When an atom absorbs a photon, the resultant oscillation amplitude is higher because the atom takes more time to absorb the photon, leading to a longer interaction time with the incident particle. This longer duration of oscillation results in less damping. In contrast, during photon emission, the atom's oscillation amplitude is lower, and the interaction time with the projected particle is shorter, resulting in higher damping in the emission case.

Figure 3 depicts the DCS as a function of varying separation distances between the target and the incident electron in a laser field. The DCS increases as the separation distance increases. For the absorption case, the DCS is notably higher, whereas for the emission case, it is lower. When the laser phase is π, the DCS reaches its peak for absorption, while it is lower for phase zero. At phase $\pi/4$, the DCS appears nearly constant due to high oscillations of the same frequency but with lower amplitude. In contrast, during emission, the DCS at phase zero shows oscillations, while at phases π and $\pi/4$, it remains constant, as illustrated in Figures 3(a) and 3(b).

At close separation distances, the DCS becomes nearly constant due to high oscillations with very low consistent amplitude. This suggests that when the target and the incident electron are very close, the Coulombic force of the target dominates over the energy of the projected particle. In this regime, the phase of the laser field has minimal impact, resulting in nearly equal DCS values across different phases. The high oscillation at close distances diminishes the influence of phase variations, leading to a uniform DCS for all phases. This behavior indicates that at small separations, the interaction is dominated by immediate electron-target dynamics, overshadowing the effects of the laser field's phase.

For ellipticity $-\pi/2$, the nature of the DCS with separation distance exhibits distinct characteristics. Specifically, at a phase of $\pi/4$, the DCS is higher than at $\pi/2$ in the elliptical case, which is contrary to the behavior observed in other cases, except for absorption scenarios. However, in emission cases, the DCS for ellipticity $-\pi/2$ surpasses that of absorption at $\pi/2$. This suggests that ellipticity plays a significant role in determining the DCS behavior. Therefore, it was important to study the DCS for all three polarization cases.

The straight line observed in the separation distance graph represents the superposition of waves, which results in reduced
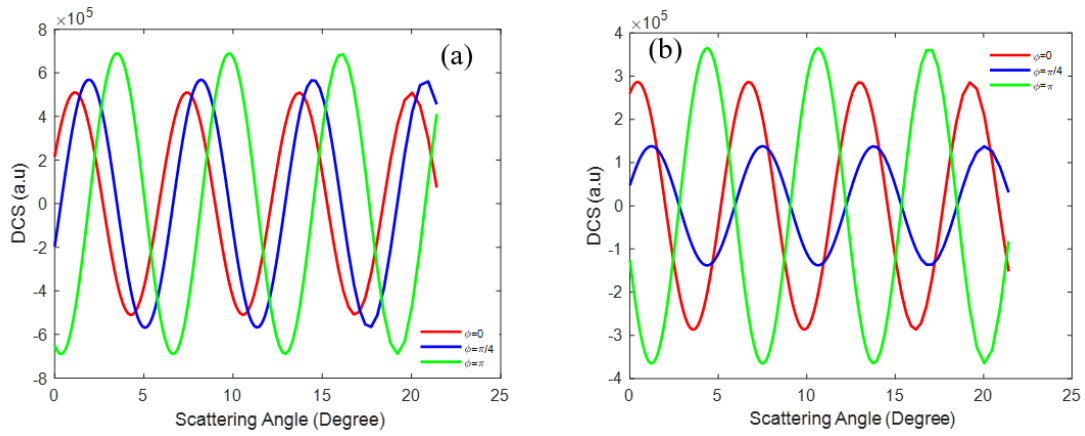
Figure 1. DCS with (a) Absorption and (b) Emission with scattering angle for $\zeta_n = \pi/2$
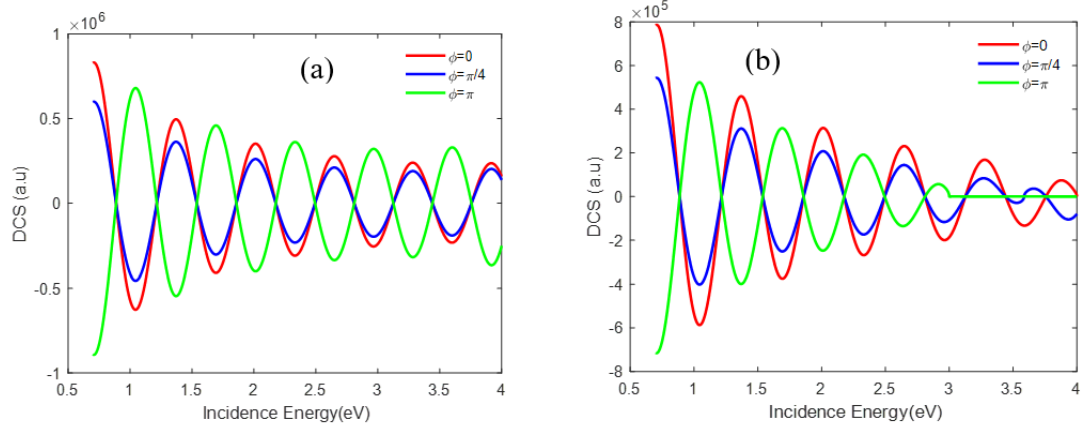
Figure 2. DCS with (a) Absorption and (b) Emission with incidence energy for $\zeta_n = \pi/2$
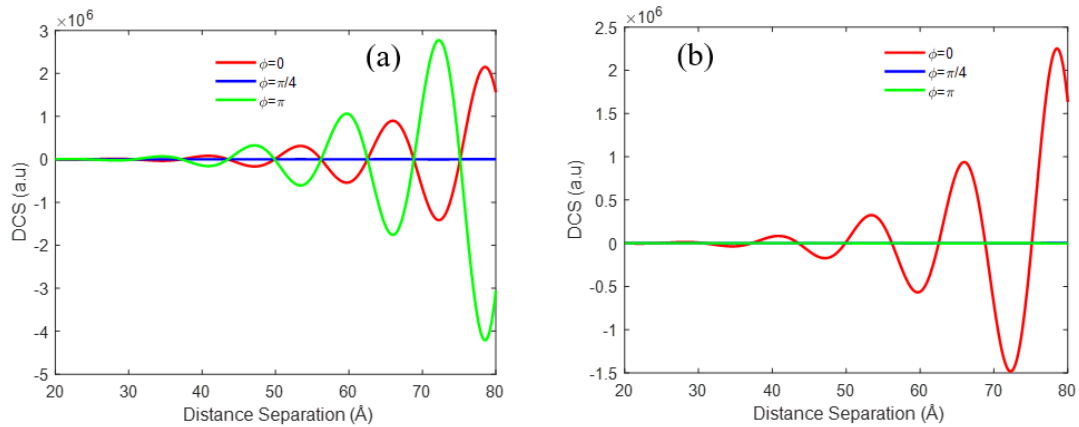
Figure 3. DCS with (a) Absorption and (b) Emission with distance separation for $\zeta_n = \pi/2$

amplitude and nearly constant DCS values. Additionally, the range of DCS values, spanning from positive to negative on the y-axis, was investigated by Ajana *et al.* [22] in their research on the second Born approximation in laser-assisted (e, 2e) collisions in hydrogen. In our study, we present both positive and negative DCS values on the axis, indicating the maximum and minimum DCS values for the interaction.

3.2. DCS for non-monochromatic linear polarization

The DCS as a function of scattering angle for the non-monochromatic linear polarization case, shown in Figure 4, exhibits trends similar to those of the non-monochromatic elliptical and non-monochromatic circular polarization cases, albeit
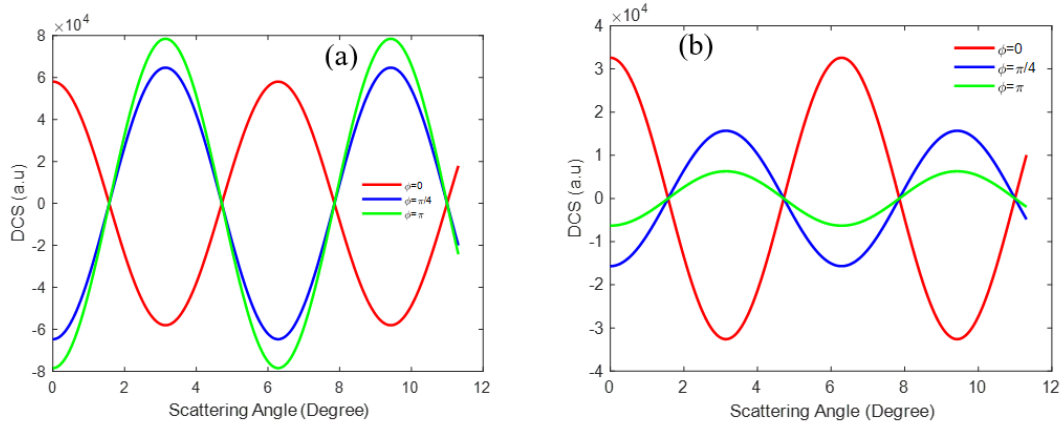
Figure 4. DCS with (a) Absorption and (b) Emission with scattering angle for $\zeta_n = 0$
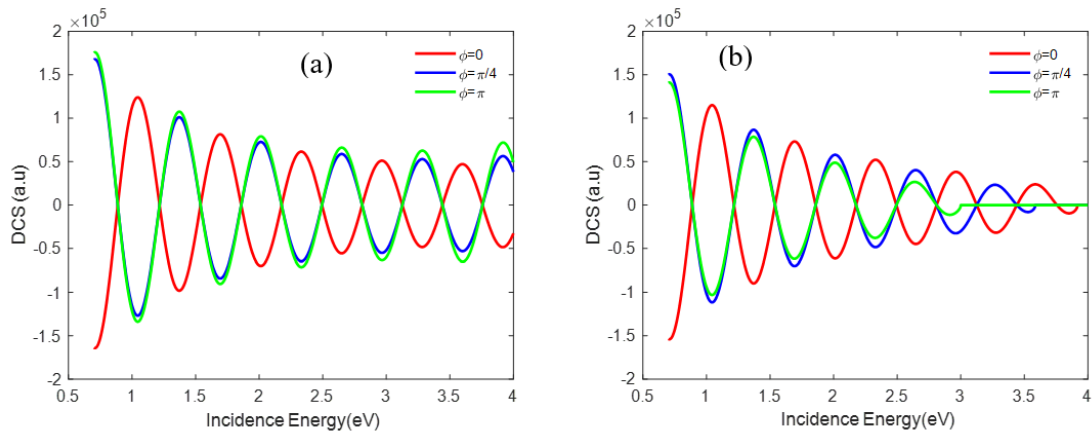

Figure 5. DCS with (a) Absorption and (b) Emission with incidence energy for $\zeta_n = 0$
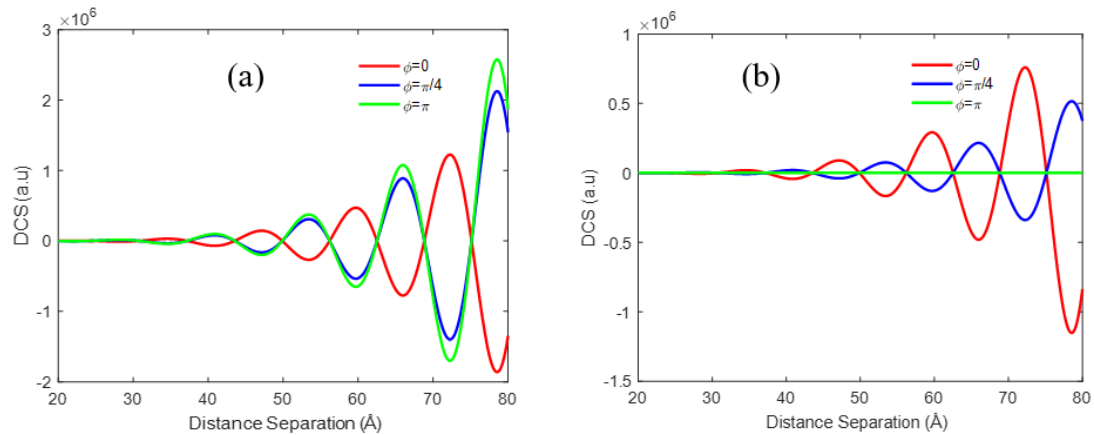

Figure 6. DCS with (a) Absorption and (b) Emission with separation distance for $\zeta_n = 0$

with differences in amplitude and the location of their maxima. In the absorption scenario, the DCS is lower for a phase of zero compared to phases $\pi/4$ and π, following an ascending order. In contrast, in the emission case, the DCS for a phase of zero is higher than for phases $\pi/4$ and π, following a descending order. This behavior arises from the interplay between absorption

and emission processes, which contribute to superpositions in the field and result in fluctuations in the DCS as a function of phase. These variations are influenced by the thermal characteristics of both the electron and the potential.

A comparison of the total double differential cross sections (TDCSs) for hydrogen ionization by electron impact in

the presence of non-monochromatic circularly polarized and non-monochromatic linearly polarized laser fields, as discussed by Buica [9], reveals a non-constant nature of the DCS for both non-monochromatic linear and non-monochromatic elliptical polarizations. Specifically, the DCS for the non-monochromatic linear case is higher at certain angles than for the non-monochromatic circular case, and vice versa at different angles. This demonstrates the dynamic nature of DCS behavior under varying polarization conditions.

Figure 5 illustrates the DCS as a function of the incidence energy of electrons for both photon absorption and emission scenarios, as shown in Figures 5(a) and 5(b), respectively. The decrease in DCS with increasing incidence energy is attributed to the Bessel function, consistent with previous findings on photon absorption [21]. As observed earlier, the DCS with scattering angle is higher at a phase of π compared to phases zero and $\pi/4$ for both emission and absorption scenarios. Additionally, the DCS for the linear polarization case is lower compared to the non-monochromatic circular and elliptical polarization cases.

In the absorption of photons, the damping of the DCS occurs more slowly, whereas in the emission case, it occurs more rapidly. This difference arises because when an atom absorbs a photon, the resultant oscillation of the thermal electron and atom takes more time, as the system gains energy, leading to a longer duration of oscillation with less damping. In contrast, during photon emission, the lower energy associated with oscillation results in the atom's inability to resist damping effectively, leading to faster damping. Thus, the dynamics of energy exchange between absorption and emission processes significantly influence the damping behavior of the DCS.

Figure 6 illustrates the DCS as a function of the separation distance between the target and the incident electron in a non-monochromatic linearly polarized laser field. The DCS increases as the separation distance increases, exhibiting a similar trend to that observed in the non-monochromatic circular and elliptical polarization cases. In the absorption scenario, the DCS is higher, while in the emission scenario, it is lower. Specifically, for absorption, the DCS is higher for a phase of π, while it is lower for phases zero and $\pi/4$, with increasing oscillations. This behavior is consistent across all three non-monochromatic polarization cases (elliptical, circular, and linear). When the separation between the target and the projected electron is minimal, highly oscillatory behavior with the same amplitude is observed, resulting in a nearly straight line. For emission, oscillations are observed at phases zero and $\pi/4$, while for phase π, the DCS remains constant due to high-frequency oscillations with consistent amplitude. Figure 6(a) depicts the absorption case for linear polarization, while Figure 6(b) illustrates the emission case.

Laser-assisted thermal processes are used to precisely heat microparticles, nanoparticles (NPs), and biological tissues [23]. Applications include laser treatment of materials, selective photothermolysis in medicine (e.g., cancer cell destruction using nanoparticles), and nanotechnologies involving plasmonic NPs for light-to-heat conversion [24]. The heating is highly localized and controlled, enabling applications in biomedical procedures, nanomaterial processing, and catalysis [25]. Thus, this design model has significant potential for thermal management at the nanoscale in various quantum systems.

4. Conclusion

In conclusion, this study explores the intricate dynamics of electron-atom interactions under the influence of non-monochromatic laser fields within a thermal environment. Through a rigorous analysis of the DCS across various scenarios, we have uncovered nuanced behaviors dictated by laser parameters, polarization, and thermal effects. The influence of laser phase, polarization direction, and separation distance between the electron and the target further modulates the DCS characteristics, revealing distinct patterns for absorption and emission scenarios. Thermal dynamics play a significant role, with slower damping observed in absorption due to energy gain and prolonged oscillations, in contrast to faster damping in emission. This comprehensive exploration extends beyond previous monochromatic studies, offering novel insights into laser-matter interactions that are crucial for quantum control and photochemistry applications. By addressing this research gap, we contribute to advancing the understanding of laser-induced processes, paving the way for future advancements in manipulating molecular dynamics and optimizing quantum control strategies.

Data Availability

No datasets were used in this study. The code used to generate the equations is available upon reasonable request from the corresponding author.

References

[1] A. D. Bandrauk & S. Chelkowski, "Asymmetric electron-nuclear dynamics in two-color laser fields: Laser phase directional control of photofragments in H_2^+", AIP Conference Proceedings **525** (2000) 547. https://doi.org/10.1063/1.1595653.

[2] J. Zhang & T. Nakajima, "Coulomb effects in photoionization of H atoms irradiated by intense laser fields", Physical Review A **75** (2007) 043403. https://doi.org/10.1103/PhysRevA.75.043403.

[3] S. Schnez, E. Lötstedt, U. D. Jentschura & C. H. Keitel, "Laser-assisted bremsstrahlung for circular and linear polarization", Physical Review A **75** (2007) 053412. https://doi.org/10.1103/PhysRevA.75.053412.

[4] F. Jin, W. Yang, X. Liu, H. Zhang, W. Dong, X. Song & J. Chen, "Control of photoelectron interference dynamics with two-color laser fields", Physical Review Research **4** (2022) 013140. https://doi.org/10.1103/PhysRevResearch.4.013140.

[5] F. Jin, Y. Tian, J. Chen, Y. Yang, X. Liu, Z.-C. Yan & B. Wang, "Nonsequential double ionization of helium in IR+XUV two-color laser fields: Collision-ionization process", Physical Review A **93** (2016) 043417. https://doi.org/10.1103/PhysRevA.93.043417.

[6] S. Yu, Y. Wang, X. Lai, Y. Huang, W. Quan & X. Liu, "Coulomb effect on photoelectron momentum distributions in orthogonal two-color laser fields", Physical Review A **94** (2016) 033418. https://doi.org/10.1103/PhysRevA.94.033418.

[7] M. Richter, M. Kunitski, M. Schoffler, T. Jahnke & L. P. H. Schmidt, "Streaking temporal double-slit interference by an orthogonal two-color laser field", Physical Review Letters **114** (2015) 143001. https://doi.org/10.1103/PhysRevLett.114.143001.

[8] G. Buica, "Dressing effects in the laser-assisted (e,2e) process in fast-electron–hydrogen-atom collisions in an asymmetric coplanar scattering geometry", Physical Review A **106** (2022) 022804. https://doi.org/10.1103/PhysRevA.106.022804.

[9] G. Buica, "Comparative study of fast-electron-impact ionization of a hydrogen atom in circularly and linearly polarized laser fields", Physical Review A **109** (2024) 052808. https://doi.org/10.1103/PhysRevA.109.052808.

[10] S. H. Dhobi, J. J. Nakarmi, K. Yadav, S. P. Gupta & B. Koirala, "Differential cross-section in the presence of a weak laser field for inelastic scattering", Ukrainian Journal of Physics **67** (2022) 227. https://doi.org/10.15407/ujpe67.4.227.

[11] S. H. Dhobi, J. J. Nakarmi, K. Yadav, S. P. Gupta, B. Koirala & A. K. Shah, "Study of thermodynamics of a thermal electron in scattering", Heliyon **8** (2022) e12315. http://dx.doi.org/10.1016/j.heliyon.2022.e12315.

[12] S. H. Dhobi, S. P. Gupta, K. Yadav, J. J. Nakarmi & A. K. Jha, "Differential cross-section with Volkov-thermal wave function in Coulomb potential", Atom Indonesia **50** (2024) 19. http://dx.doi.org/10.55981/aij.2024.1309.

[13] D. B. Milosevic, "Potential scattering in a strong multicolour laser field", Journal of Physics B: Atomic, Molecular and Optical Physics **29** (1996) 875. http://dx.doi.org/10.1088/0953-4075/29/4/024.

[14] S. Luo, M. Li, H. Xie, P. Zhang, S. Xu, Y. Li, Y. Zhou, P. Lan & P. Lu, "Angular-dependent asymmetries of above-threshold ionization in a two-color laser field", Physical Review A **96** (2017) 023417. https://doi.org/10.1103/PhysRevA.96.023417.

[15] F. Ehlotzky, "Atomic phenomena in bichromatic laser fields", Physics Reports **345** (2001) 175. https://doi.org/10.1016/s0370-1573(00)00100-9.

[16] J. Maurer & U. Keller, "Ionization in intense laser fields beyond the electric dipole approximation: Concepts, methods, achievements and future directions", Journal of Physics B: Atomic, Molecular and Optical Physics **54** (2021) 094001. https://doi.org/10.1088/1361-6455/abf731.

[17] D. Solovyev, T. Zalialiutdinov & A. Anikin, "Relativistic corrections to the thermal interaction of bound particles," Physical Review Research **3** (2021) 023102. https://doi.org/10.1103/PhysRevRes.3.023102.

[18] G. Buica, "Inelastic scattering of electrons by metastable hydrogen atoms in a laser field", Physical Review A **92** (2015) 033421. https://doi.org/10.1103/PhysRevA.92.033421.

[19] B. A. De Harak, B. N. Kim, C. M. Weaver, N. L. S. Martin & M. Siavashpouri, "Effects of polarization direction on laser-assisted free-free scattering", Plasma Sources Science and Technology **25** (2016) 035021. https://doi.org/10.1088/0953-4075/25/3/035021.

[20] A. Jablonski, F. Salvat & C. J. Powell, "Comparison of electron elastic-scattering cross sections calculated from two commonly used atomic potentials", Journal of Physical and Chemical Reference Data **33** (2004) 409. https://doi.org/10.1063/1.1595653.

[21] A. Makhoute, H. Agueny, A. Dubois, I. Ajana & A. Taoutioui, "Electron-impact elastic scattering of helium in the presence of a laser field: Nonperturbative approach", Journal of Physics B: Atomic, Molecular and Optical Physics **49** (2016) 075204. https://doi.org/10.1088/0953-4075/49/7/075204.

[22] I. Ajana, A. Makhoute, D. Khalil & A. Dubois, "The second Born approximation in laser-assisted (e, 2e) collisions in hydrogen", Journal of Physics B: Atomic, Molecular and Optical Physics **47** (2014) 175001. https://doi.org/10.1088/0953-4075/47/17/175001.

[23] V. K. Pustovalov, "Heating of nanoparticles and their environment by laser radiation and applications", Nanotechnology and Precision Engineering **7** (2024) 2. https://doi.org/10.1063/10.0022560.

[24] V. P. Zharov, V. Galitovsky & M. Viegas, "Photothermal detection of local thermal effects during selective nanophotothermolysis", Applied Physics Letters **83** (2003) 4897. https://doi.org/10.1063/1.1632546.

[25] R. R. Anderson & J. A. Parrish, "Selective photothermolysis: Precise microsurgery by selective absorption of pulsed radiation", Science **220** (1983) 524. https://doi.org/10.1126/science.6836297.